

# One-dimensional disorder in $Zr_9M_{11}$ ( $M = Ni, Pd, Pt$ ) and low-temperature atomic mobility in $Zr_9Ni_{11}$

J K Stalick<sup>1</sup>, L A Bendersky<sup>2</sup> and R M Waterstrat<sup>2</sup>

<sup>1</sup> NIST Center for Neutron Research, National Institute of Standards and Technology, Gaithersburg, MD 20899, USA

<sup>2</sup> Materials Science and Engineering Laboratory, National Institute of Standards and Technology, Gaithersburg, MD 20899, USA

Received 14 March 2008, in final form 17 March 2008

Published 17 June 2008

Online at [stacks.iop.org/JPhysCM/20/285209](http://stacks.iop.org/JPhysCM/20/285209)

## Abstract

The  $Zr_9M_{11}$  structure type ( $M = Ni, Pd, Pt$ ) has been investigated using transmission electron microscopy and powder neutron diffraction in the temperature range 4–1273 K. The crystal structures are tetragonal,  $P4/m$ ,  $Z = 2$ , with  $a = 9.882(1)$  Å,  $c = 6.6089(5)$  Å for  $M = Ni$ ,  $a = 10.313(1)$  Å,  $c = 6.9405(5)$  Å for  $M = Pd$ , and  $a = 10.356(1)$  Å,  $c = 6.913(1)$  Å for  $M = Pt$  at room temperature. At 1273 K the structure of  $Zr_9Ni_{11}$  is body-centered  $I4/m$ . These materials have a host periodic structure, which is derived from the B2 structure type by insertion of anti-site M atoms, with structurally disordered one-dimensional chains of Zr and M atoms that are only weakly correlated with each other. For  $Zr_9Ni_{11}$ , it was found that additional M (Ni) atoms are inserted in these chains to give a composition of  $Zr_9Ni_{11+\delta}$  ( $\delta \approx 0.4$ ). The diffuse scattering from the chains results in two-dimensional sheets of intensity in reciprocal space with translations which are in general incommensurate with the translations of the host lattice. These chains form within open channels along the tetragonal fourfold axes, and the atoms within the chains are apparently mobile over short distances at temperatures down to 4 K.

## 1. Introduction

One-dimensional structures containing interacting electrons are a subject of intense interest because of their importance to such things as nanotubes, semiconductor quantum wire structures, one-dimensional organic superconductors, low dimensional magnets, and cuprate superconductors. In diffraction experiments, deviations of atoms from an ideal crystal structure (positional disorder) may cause the replacement of intensity localized in Bragg positions by diffuse intensity. A classification scheme for different types of disorder, ranging from an amorphous glass to a perfect crystal, was derived by Hermann in 1931 using group theory [1]. Mabis [2] has provided illustrations of these eighteen different structural types in real and reciprocal space. In particular, the diffuse scattered intensity appears in the form of equidistant planes (or sheets) in reciprocal space when molecular centers are spaced at equal intervals along parallel lines but the linear displacement of lines relative to one another is random.

In this paper we present examples of one-dimensional structural disorder in the intermetallic compounds  $Zr_9M_{11}$  ( $M = Ni, Pd, Pt$ ). These materials have previously been studied using x-ray powder diffraction. The structure of the type compound,  $Zr_9Pt_{11}$ , was reported by Panda and Bhan [3] to be tetragonal with a body-centered ( $I$ -centered) lattice, space group  $I4/m$ , with  $a = 10.297$  Å and  $c = 6.888$  Å. The atoms on the fourfold symmetry axes were reported to occupy the positions 2a (0, 0, 0) for the Zr atoms and 2b (0, 0, 1/2) for the Pt atoms. A similar  $I$ -centered lattice was reported for  $Zr_9Ni_{11}$  by Kirkpatrick and Larsen [4] in 1961, and the structure subsequently was shown to be isomorphous with  $Zr_9Pt_{11}$  with  $a = 9.88(1)$  Å and  $c = 6.61(1)$  Å [5, 6]. Preparation of the isostructural compound  $Zr_9Pd_{11}$  was reported by Waterstrat *et al* [7] in 1999 with  $a = 9.90$  Å and  $c = 6.62$  Å. Here we report structural results for these compounds derived from analysis of transmission electron microscopy and powder neutron diffraction data.

## 2. Experimental details

### 2.1. Sample preparation

All samples were arc-melted four times and then arc-cast into a 1/4-in diameter rod in a water-cooled copper mold. Annealing treatments were as follows:  $Zr_9Pt_{11}$ , 1200 °C for 1.5 h;  $Zr_9Pd_{11}$ , 900 °C for two weeks;  $Zr_9Ni_{11}$ , 1030 °C for one week, water quenched.

### 2.2. Transmission electron microscopy (TEM)

TEM specimens were prepared from the bulk ingots by slicing, thinning, and ion-milling. These samples were characterized both by selected-area electron diffraction (SAED) and convergent-beam analysis. Electron diffraction of these Zr-containing materials typically showed thickness-dependent intensity in the form of arcs which we attribute to surface damage due to ion-milling. A similar phenomenon was observed in our previous work with different Zr–Pd alloys [8, 9].

### 2.3. Neutron diffraction

Neutron diffraction data were collected using the BT-1 32-detector powder diffractometer at the NIST Center for Neutron Research. Data were collected on  $Zr_9Pt_{11}$ ,  $Zr_9Pd_{11}$ , and  $Zr_9Ni_{11}$  using the Cu(311) monochromator with a take-off angle of 90° and a wavelength of 1.5400(1) Å or 1.5403(1) Å. The in-pile collimation used was 15' of arc. Data were collected over the range 3° 2 $\theta$  to 168° 2 $\theta$  with a step size of 0.05°. High-temperature data in the range 500–1000 °C were obtained using a vacuum furnace with a Nb heating element, with the sample suspended by W–Re wire. For low-temperature data collection, the samples were placed in a He-filled vanadium can, using a He-filled cryostat for temperature control down to 1.4 K or a closed-cycle refrigerator for temperatures down to 3.7 K. In all cases samples were held at temperature until no further changes were observed in the diffraction pattern prior to data collection. This time was typically 3–6 h. Data were also collected during temperature changes in order to assess structural equilibrium through comparison of intensities in the overlapping regions of adjacent detectors. The crystallographic structural parameters and phase fractions were refined using the Rietveld technique as implemented in the GSAS suite of programs [10].

## 3. Results

### 3.1. TEM analysis

**3.1.1.  $Zr_9Pt_{11}$ .** The tetragonal phase was observed in the  $Zr_9Pt_{11}$  specimen annealed at 1200 °C for 1 1/2 h. Other heat treatments of the  $Zr_9Pt_{11}$  specimen resulted in different phases, which is a consequence of compositional inhomogeneity of the cast sample and the existence of a number of Zr–Pt compounds with close compositions. In fact, the complete disappearance of this tetragonal phase has been reported after long annealing at 1200 °C, indicating its metastability [11].

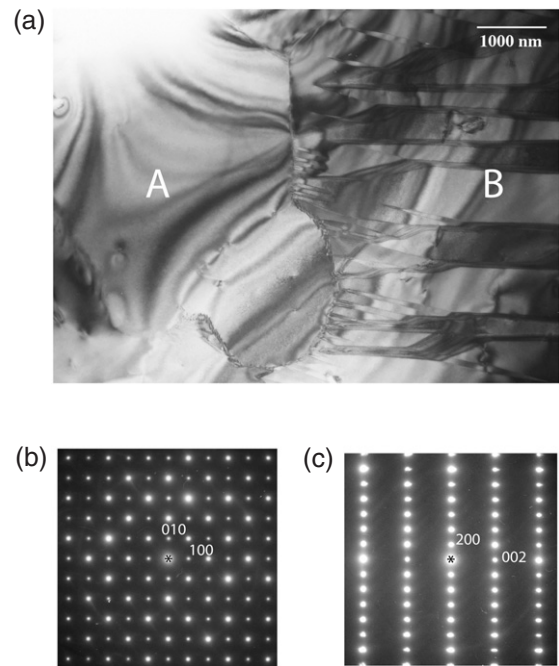


**Figure 1.** (a) TEM bright field image of the 1200 °C annealed  $Zr_9Pt_{11}$  sample showing the coexistence of two types of grains, one with a uniform contrast (labeled as A) and another with an internal domain structure and zig-zagging interfaces (labeled as B); (b) [001] SAED pattern of the tetragonal  $Zr_9Pt_{11}$  (type A) phase; (c) [010] SAED pattern of the orthorhombic (type B) phase.

The bright field image of the sample annealed for 1 1/2 h (figure 1(a)) shows the coexistence of two types of grains, one with a uniform contrast typical for a single crystal (labeled as A) and another with an internal structure of zig-zagging interfaces (labeled as B). According to SAED patterns taken at different orientations of the grains, the two grains have different crystallographic structures. Type A was identified as the tetragonal  $Zr_9Pt_{11}$  phase (figure 1(b)) whereas type B was identified by both SAED and convergent-beam patterns as having an orthorhombic lattice, with  $a = 27.6$  Å,  $b = 13.8$  Å,  $c = 9.4$  Å (figure 1(c)). Although the identified lattice does not fit any of the known Zr–Pt phases, it is most likely the  $Zr_3Pt_4$  phase that has been described as a triclinic distortion of the rhombohedral  $Zr_3Pd_4$ -type structure [11]. This phase is rhombohedral above  $\approx 100$  °C, and the presence of interfaces in the TEM bright field image is consistent with transformation from a higher symmetry to a lower symmetry structure.

The SAED pattern of the tetragonal (type A) phase in figure 1(b) fits well the [001] zone axis of  $Zr_9Pt_{11}$  ( $a = 10.29$  Å;  $c = 6.9$  Å). However, the presence of 100 and 010 reflections suggests that the structure has a Bravais lattice which is primitive and not  $I$ -centered as reported by Panda and Bhan [3]. Tilting of the tetragonal phase around the [100] (or [010]) axis also revealed the presence of diffuse broad lines running parallel to the [100] (or [010]) direction (figure 2). Intensity along the diffuse lines is modulated. Closer inspection suggests that the broad lines are in fact pairs of closely spaced lines. The distance of the lines from the origin changed with tilt angle; the shift is consistent with the interpretation that the lines result from the intersection

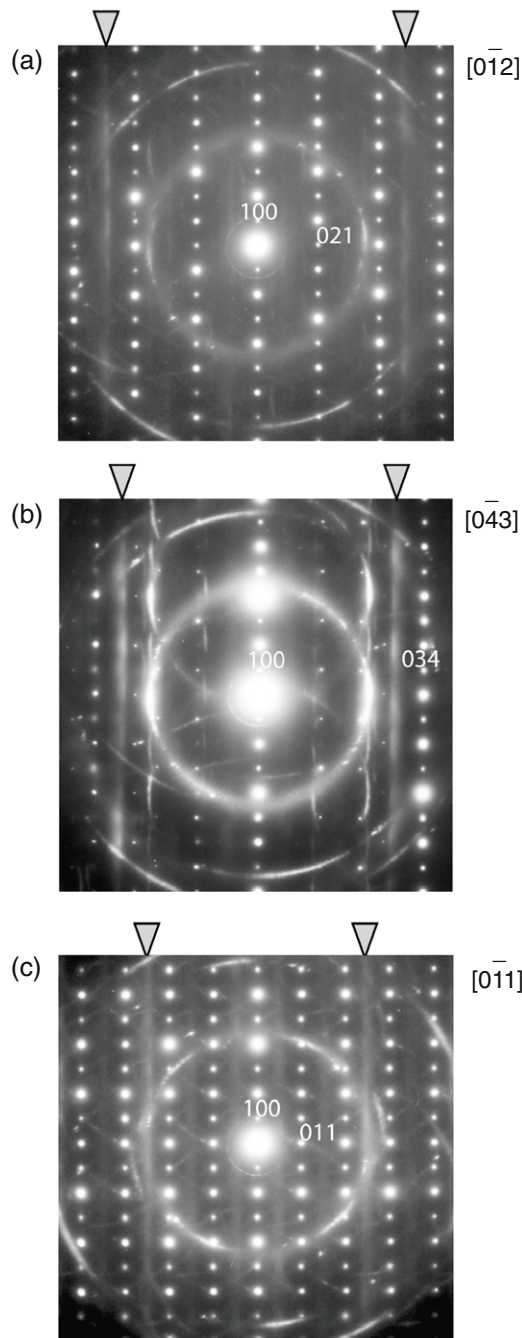


**Figure 2.** A series of SAED patterns taken from a single grain of  $Zr_9Pt_{11}$  by tilting around  $[100]^*$  reciprocal direction (zone axes  $[0\bar{1}2]$ ,  $[0\bar{4}3]$  and  $[0\bar{1}1]$ ). Arrows show the changing positions of diffuse lines. Diffuse arcs and rings of intensity around central and strong 400 spots arise from a surface layer damaged by ion-milling.

of sheets of intensity with the Ewald sphere. The sheets are parallel to (001); taking into consideration dynamic scattering, we concluded that the pairs of lines result from double scattering from systematic rows of reflections, and without this effect the first (closest to the origin) sheet of intensity is at a distance of approximately  $k_s = 2.4k_{(001)}$  from the origin.

**3.1.2.  $Zr_9Ni_{11}$ .** SAED patterns from the  $Zr_9Ni_{11}$  specimen show that it has a structure similar to  $Zr_9Pt_{11}$ . Figure 3 shows

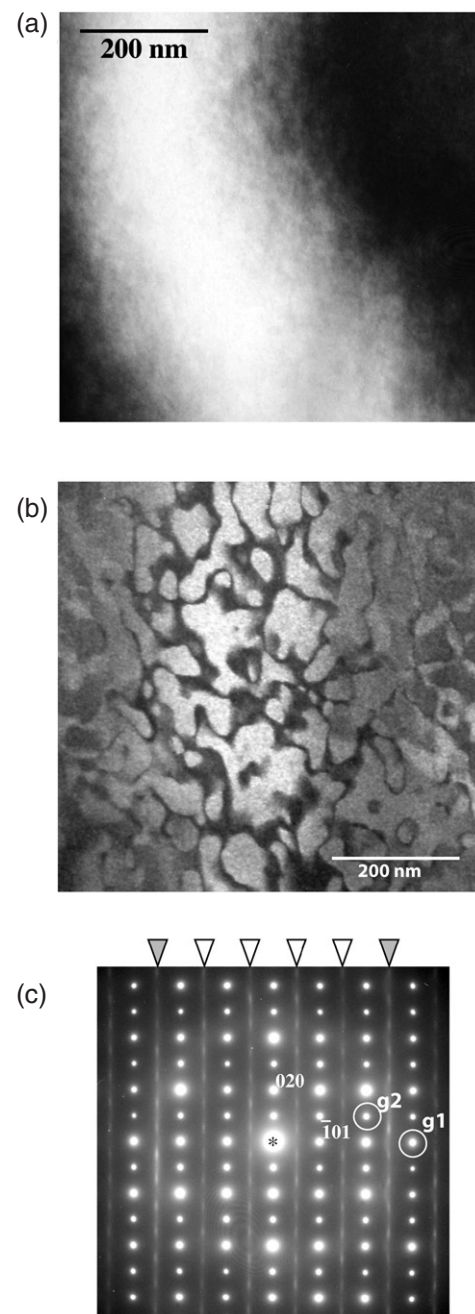


**Figure 3.** ((a), (b)) Two TEM dark field images and (c)  $[101]$  SAED pattern from a single grain of  $Zr_9Ni_{11}$ . Arrows at the top of the SAED pattern indicate the diffuse lines; the white arrows show lines which are due to double scattering.

two dark field images and a corresponding SAED pattern from a grain at  $[101]$  orientation. The image in figure 3(a) was obtained using  $g_1 = \bar{3}03$  reflection that is allowed for the  $I4/m$  space group, and its contrast is rather uniform. The image in figure 3(b) was obtained with  $g_2 = \bar{2}12$  reflection, which is forbidden for  $I4/m$ , and it shows a contrast typical for the interfaces between anti-phase domains. Anti-phase domains are regions of the same crystallographic structure which differ by a relative translation (a part of a full lattice translation). The topology of the anti-phase boundaries suggests a two-domain

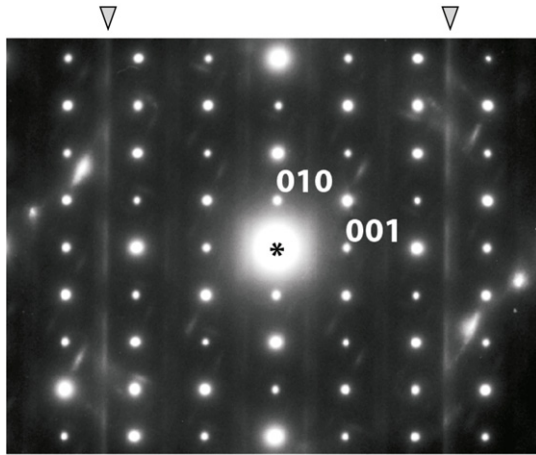


**Figure 4.** [100] SAED pattern of  $Zr_9Pd_{11}$  showing diffuse lines in the [010] direction. Intensity along the lines is modulated.

structure, and it is consistent with ordering which changes the  $I4/m$  space group to  $P4/m$  (similar to the well-studied bcc-to-B2(CsCl) ordering in many alloys, e.g. FeAl) [12]. Considering the size of the domains, the ordering apparently occurred during post-annealing cooling of the sample.

The [101] SAED pattern shows the presence of diffuse lines which are similar to those observed for  $Zr_9Pt_{11}$  (figure 3(c)). Observation of diffuse lines in other SAED patterns yields the same conclusion as was reached for  $Zr_9Pt_{11}$ —the presence of diffuse sheets parallel to (001). In the case of  $Zr_9Ni_{11}$  the lines appear to be without pairing and the distance of the first sheet from the origin is nearly commensurate with the  $c$ -axis with  $\mathbf{k}_s = 2.5\mathbf{k}_{(001)}$ .

**3.1.3.  $Zr_9Pd_{11}$ .** The TEM results for  $Zr_9Pd_{11}$  were similar to those found for  $Zr_9Pt_{11}$  and  $Zr_9Ni_{11}$ : a primitive  $P4/m$  space group, the presence of anti-phase domains, and sheets of diffuse intensity running parallel to (001). The [100] SAED pattern (figure 4) shows doubled diffuse lines aligned in [010]. Similar to  $Zr_9Pt_{11}$ , when double diffraction effects of dynamic scattering are taken into account we conclude that the sheets are single and that the first sheet of intensity is at  $\mathbf{k}_s = 2.45\mathbf{k}_{(001)}$  from the origin. Judging from the non-uniform distribution of intensity along the diffuse lines for different orientations, we also observe that intensity along the sheets is not uniform but two-dimensionally modulated with periodicities of the (001) crystallographic plane.

### 3.2. Phase composition from neutron Rietveld refinement

**3.2.1.  $Zr_9Pt_{11}$ .** As determined from the Rietveld refinement, the  $Zr_9Pt_{11}$  sample consisted of approximately 60% tetragonal phase and 40% of a lower symmetry phase which has been reported as  $Zr_3Pt_4$  [11]. The structure of this lower symmetry phase was approximated as a triclinic distortion of the rhombohedral  $Zr_3Pd_4$ -type structure for the Rietveld structural refinement although a larger orthorhombic unit cell was indicated by the SAED patterns (see above). Refinement results are presented in table 1.

**Table 1.** Neutron Rietveld refinement results. Standard uncertainties are given in parentheses.

Compound <sup>a</sup>	$T$ (K)	Space		$a$ (Å)	$c$ (Å)	$\chi^2$	$R_{wp}$	$d_s$ <sup>b</sup>
		group	$Z$					
$Zr_9Ni_{11}$	10	$P4/m$	2	9.865(1)	6.5988(5)	1.6	6.2	2.64
	293	$P4/m$	2	9.882(1)	6.6089(5)	1.1	3.9	
	1273	$I4/m$	2	10.000(1)	6.6792(5)	2.1	4.2	
$Zr_9Pd_{11}$	293	$P4/m$	2	10.313(1)	6.9405(5)	1.6	8.1	2.83
$Zr_9Pt_{11}$	293	$P4/m$	2	10.356(1)	6.913(1)	2.8	7.7	2.88

<sup>a</sup> The  $Zr_9Ni_{11}$  sample consisted of a mass fraction of 90%  $Zr_9Ni_{11}$  and 10% ZrNi with the CrB structure type.  $Zr_9Pd_{11}$  had a small amount of an unidentified second phase, and the  $Zr_9Pt_{11}$  sample consisted of a mass fraction of 60%  $Zr_9Pt_{11}$  and 40%  $Zr_3Pt_4$ .

<sup>b</sup>  $d_s$  represents the spacing of the diffuse sheets parallel to the (001) plane as determined from the SAED data, where  $\mathbf{k}_s = 2.5\mathbf{k}_{(001)}$  for  $Zr_9Ni_{11}$ ,  $\mathbf{k}_s = 2.45\mathbf{k}_{(001)}$  for  $Zr_9Pd_{11}$  and  $\mathbf{k}_s = 2.4\mathbf{k}_{(001)}$  for  $Zr_9Pt_{11}$ .

**3.2.2.  $Zr_9Ni_{11}$ .** Rietveld refinement using the neutron diffraction data for  $Zr_9Ni_{11}$  indicated a mass fraction of 10% ZrNi (CrB structure type;  $Cmcm$ ,  $a = 3.2687(3)$ ,  $b = 9.943(1)$ ,  $c = 4.1121(4)$  Å) as a second phase in addition to the primary tetragonal phase. Refinements using data taken at high temperature showed that by 700 °C the sample had transformed to approximately 37% ZrNi, 57%  $Zr_7Ni_{10}$ , and 7%  $Zr_9Ni_{11}$ , and that the tetragonal  $Zr_9Ni_{11}$  phase re-formed at 1000 °C so that the sample was again 90%  $Zr_9Ni_{11}$  and 10% ZrNi. Upon cooling in the furnace the tetragonal phase was retained at 600 °C down to room temperature. A summary of the results of the Rietveld refinements at 10, 293, and 1273 K is given in table 1.

**3.2.3.  $Zr_9Pd_{11}$ .** The  $Zr_9Pd_{11}$  sample consisted of a tetragonal phase isostructural with  $Zr_9Pt_{11}$  and  $Zr_9Ni_{11}$  along with approximately 5% of a second unidentified phase. Data were also collected upon heating; the 9:11 tetragonal phase persisted to approximately 1173 K. Above 1173 K this phase disproportionated to form a B2-type phase (presumably ZrPd) and the rhombohedral  $Zr_3Pd_4$  phase [8]; a complex mixture of phases was obtained upon cooling to room temperature. Table 1 gives a summary of the refinement results.

The complexity of the mixed phases for  $Zr_9Pt_{11}$  and the presence of an unknown phase for  $Zr_9Pd_{11}$  made a detailed analysis of these data sets unrewarding. Only the  $Zr_9Ni_{11}$  sample, with the easily-characterized ZrNi second phase, was subjected to detailed structural analysis.

### 3.3. Structural analysis of $Zr_9Ni_{11}$

Data were collected at room temperature after two months and again after two years, and refinement results were similar to those from the original data with some slight differences in intensities but no statistically significant changes in refined structural parameters. Data were also subsequently collected at 1273 K (1000 °C) and at several temperatures down to 1.4 or 3.7 K. Several experiments involving cooling in a closed-cycle He refrigerator resulted in quite variable relative integrated intensities from one experiment to the next, particularly for the two strongest reflections of the neutron pattern indexed as

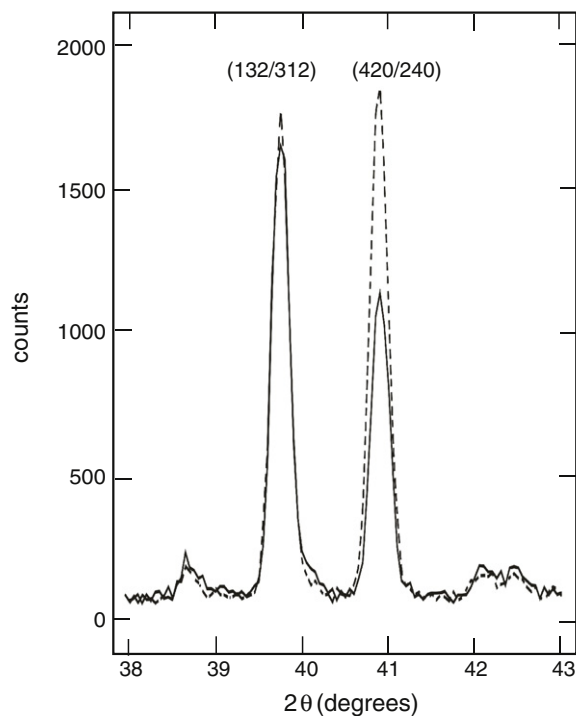


**Figure 5.** Portion of the neutron diffraction pattern of  $Zr_9Ni_{11}$  at 10 K showing overlap region of two detectors after 1 h (---) and 2.5 h (—) of data collection; sample had been held at 4 K overnight. Error bars, not shown, are commensurate with indicated scatter.

the (132/312) near  $39.6^\circ 2\theta$  and the (420/240) near  $40.8^\circ 2\theta$  based on a tetragonal unit cell. Whereas the intensity of the (132/312) reflection remained essentially constant, the ratio of the intensities (132/312) to (420/240) varied from 2.2 down to 1.2. In one experiment this ratio was transiently (at least for several minutes) 0.9, approximately 1 h after the sample temperature was raised to 10 K after being held below 4 K overnight (see figure 5); in a previous experiment the ratio was close to 1.2 in the entire temperature range 4–300 K. After 2.5 h at 10 K the ratio was close to 1.4 where it remained as the temperature was raised to 300 K. In subsequent experiments on different days the phenomenon of transient changes in intensity was again exhibited in the 4 to 10 K region, as well as at temperatures up to 90 K, although not as dramatically. When the sample was subsequently cooled in a He-filled cryostat, no transient intensity changes were observed; however, the intensity ratio of the (132/312) to (420/240) reflections increased to 2.4 at 1.5 K and 2.5 at 10 K.

Refinement of the crystal structure at room temperature confirms that the space group, as indicated by the SAED data, is  $P4/m$  rather than  $I4/m$  as reported previously [3]. The additional reflections permitted by the primitive space group are obvious, and profile agreement parameters are significantly improved (for  $P4/m$ ,  $\chi^2 = 1.1$  and  $R_{wp} = 3.9$ ; for  $I4/m$ ,  $\chi^2 = 4.4$  and  $R_{wp} = 7.9$ ). Although it is not possible to assign definitive positions to the Ni and Zr atoms occupying the channels along the two crystallographically independent fourfold axes at  $(0, 0, z)$  and  $(1/2, 1/2, z)$ , both difference Fourier mapping and bond distance calculations indicate that occupancy of certain positions is preferred and that these

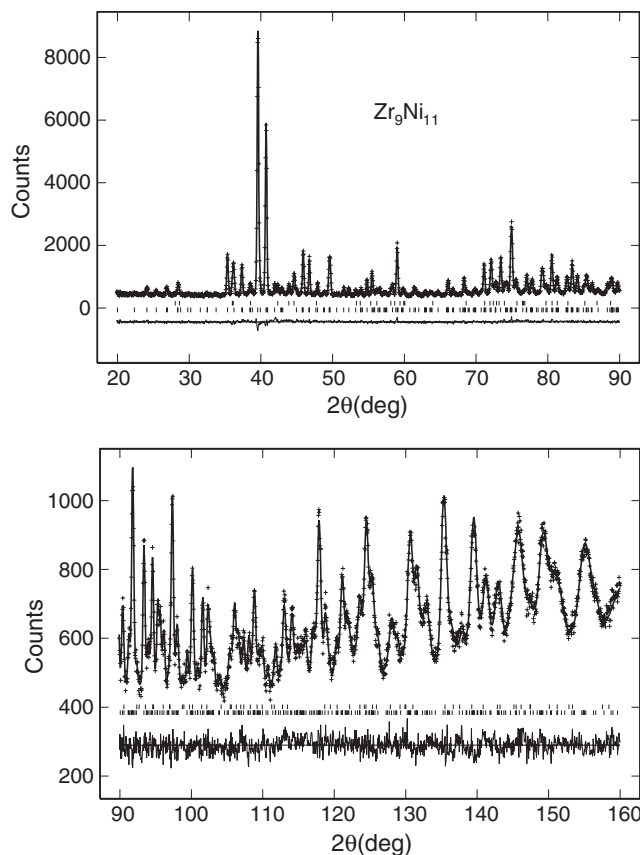


**Figure 6.** Observed (+), calculated (solid line), and difference neutron patterns for  $Zr_9Ni_{11}$  at room temperature. The tic marks indicate the calculated positions for the  $ZrNi$  (upper set) and  $Zr_9Ni_{11}$  (lower set) reflections.

positions are different for the two fourfold axes. We therefore modeled the channel sites with fractional occupancies for the Zr and Ni atoms lying off of the crystallographic mirror planes, with the Zr atoms occupying the sites with the larger atomic contact distances. The channel atoms were refined with anisotropic thermal parameters, resulting in large values for  $u_{33}$ , in order to better fit the data. However, these thermal parameters are not considered meaningful except as an indication of static disorder along the  $c$ -axis. Refinement results are given in table 2; the agreement between the calculated and observed neutron intensities is given in figure 6.

Rietveld refinement of the structure for one of the data sets collected at 10 K in a He-filled cryostat gave results similar to those for the room-temperature data, with the exception of reduced values for the  $u_{33}$  thermal parameters for the atoms along the fourfold axes. In particular, the Zr and Ni atoms on the axis at  $x, y = 1/2, 1/2$  appear to occupy significantly more localized positions based upon these values (see table 2).

The neutron pattern at  $1000^\circ C$  does not exhibit the extra reflections from the primitive lattice, although the CrB-type  $ZrNi$  phase remains. We therefore refined this structure in the space group  $I4/m$ . However, again the locations of the Zr and Ni atoms in the channel along the fourfold symmetry axis do not appear to be entirely randomized, and locating the atoms with fractional occupancy off of the positions at

**Table 2.** Atomic coordinates for  $Zr_9Ni_{11}$  at 293 and at 10 K. Space group  $P4/m$ ; standard uncertainties are given in parentheses.

Atom	Site	$T$ (K)	$x$	$y$	$z^a$	Occupancy	$U_{iso}$ or $u_{33}^a$ ( $\text{\AA}^2$ )
Zr(1)	2h	293	1/2	1/2	0.720(6)	0.5	0.28(4) <sup>a</sup>
		10	1/2	1/2	0.640(4)	0.5	0.11(2)
Zr(2)	2g	293	0	0	0.089(2)	0.5	0.014(5) <sup>a</sup>
		10	0	0	0.066(2)	0.5	0.017(6)
Zr(3)	4k	293	0.5978(5)	0.7968(5)	1/2	1.0	0.014(1)
		10	0.5972(5)	0.7962(6)	1/2	1.0	0.013(1)
Zr(4)	4j	293	0.0778(4)	0.3214(4)	0	1.0	0.005(1)
		10	0.0739(5)	0.3229(5)	0	1.0	0.006(1)
Zr(5)	4k	293	0.9272(4)	0.7492(5)	1/2	1.0	0.015(1)
		10	0.9292(5)	0.7483(6)	1/2	1.0	0.014(1)
Zr(6)	4j	293	0.4123(5)	0.2685(4)	0	1.0	0.011(1)
		10	0.4109(6)	0.2636(6)	0	1.0	0.014(1)
Ni(1)	2h	293	1/2	1/2	0.846(3)	0.5	0.14(1) <sup>a</sup>
		10	1/2	1/2	0.859(2)	0.5	0.05(1)
Ni(2)	2g	293	0	0	0.320(2)	0.5	0.033(5) <sup>a</sup>
		10	0	0	0.308(1)	0.5	0.013(4)
Ni(3)	4i	293	1/2	0	0.7111(5)	1.0	0.0111(4)
		10	1/2	0	0.7160(5)	1.0	0.0029(4)
Ni(4)	8l	293	0.7403(2)	0.6160(2)	0.7098(3)	1.0	0.0105(2)
		10	0.7424(2)	0.6166(2)	0.7080(3)	1.0	0.0062(2)
Ni(5)	8l	293	0.2188(2)	0.1265(2)	0.2032(3)	1.0	0.0140(2)
		10	0.2163(2)	0.1250(3)	0.2017(3)	1.0	0.0109(3)

<sup>a</sup> The atoms on the fourfold axes at  $x, y = 0, 0$  and  $1/2, 1/2$  were refined anisotropically; owing to strong correlations among the thermal parameters the values for  $u_{11}$  and  $u_{22}$  were fixed at  $0.01 \text{\AA}^2$  at 293 K and  $0.005 \text{\AA}^2$  at 10 K. The  $z$  coordinates for these atoms for are not well defined (see text).

$(0, 0, 0)$  and  $(0, 0, 1/2)$  gave much better agreement between calculated and observed intensities. To confirm further this body-centered structure, a refinement was carried out in  $P4/m$  starting with the atomic positions from the room-temperature data. All atoms shifted during refinement so that the coordinates for each atom agreed with the equivalent atom at the body-centered position  $(x, y, z + 1/2, 1/2, 1/2)$  within three standard uncertainties, and the agreement factors were identical with those for the body-centered refinement in  $I4/m$ . Refinement results are given in table 3. The neutron structural refinements confirm the transformation upon cooling from a body-centered lattice to a primitive lattice as was indicated by the SAED patterns.

### 3.4. Stoichiometry

It has been reported that the stoichiometry of  $Zr_9Ni_{11}$  is actually closer to  $Zr_{8.85}Ni_{11.15}$  [13], which corresponds to a composition of  $Zr_9Ni_{11.34}$ . This Ni-rich composition is supported by our observation that the sample prepared at the 9:11 atomic ratio contained a mass fraction of 10% ZrNi as a second phase. The Ni-rich composition could result from Zr vacancies, chemical substitution of Ni atoms for Zr atoms, or by ‘stuffing’ additional Ni atoms into the structure. The structural refinements indicate that it is highly unlikely that any of these would occur within the Zr–Ni framework; thus we assume that any deviations from the ideal composition would occur within the Zr–Ni chains along the fourfold axes.

Accordingly, Rietveld refinements of the structural parameters at 10, 293, and 1273 K were performed assuming additional scattering density on the fourfold symmetry axes.

**Table 3.** Atomic coordinates for  $Zr_9Ni_{11}$  at 1273 K (1000 °C). Space group  $I4/m$ ; standard uncertainties are given in parentheses.

Atom	Site	$x$	$y$	$z^a$	Occupancy	$U_{iso}$ ( $\text{\AA}^2$ ) <sup>a</sup>
Zr(1)	4e	0	0	0.108(4)	0.5	
Zr(2)	8h	0.4177(6)	0.2528(6)	0	1.0	0.051(1)
Zr(3)	8h	0.0825(5)	0.3069(6)	0	1.0	0.041(1)
Ni(1)	4e	0	0	0.321(2)	0.5	
Ni(2)	4d	0	1/2	1/4	1.0	0.064(2)
Ni(3)	16i	0.2279(3)	0.1204(2)	0.2080(3)	1.0	0.049(1)

<sup>a</sup> The atoms on the fourfold axis at  $x, y = 0, 0$  were refined anisotropically. For Zr(1),  $u_{11} = u_{22} = 0.06(1) \text{\AA}^2$  and  $u_{33} = 0.07(1) \text{\AA}^2$ ; for Ni(1),  $u_{11} = u_{22} = 0.032(4) \text{\AA}^2$  and  $u_{33} = 0.11(1) \text{\AA}^2$ . The  $z$ -coordinates are not well defined owing to the disorder along this axis.

The added density was assumed to be from Ni atoms, and the resulting fractional occupancies are given in table 4. All three refinements indicate the presence of additional scattering density equivalent to approximately 0.8(1) additional Ni atoms per unit cell, giving a composition of  $Zr_9Ni_{11.4}$  which is in good agreement with the composition of  $Zr_9Ni_{11.34}$  reported by Joubert *et al* [13]. In all three refinements the agreement between calculated and observed patterns was significantly improved. The channel along the fourfold axis at  $x, y = 0, 0$  can thus accommodate one additional Ni atom for approximately every two unit cell distances. This addition, along with small shifts in the positions of the original Zr and Ni atoms, would result in extended –Zr–Ni–Zr–Ni–Ni–Zr–Ni–Zr–Ni–Ni–rods that extend across the commensurate lattice. The channel along the fourfold axis at  $x, y = 1/2, 1/2$  has

**Table 4.** Fractional occupancies of potential Ni sites in  $Zr_9Ni_{11}$ .

Space group	Site	$x$	$y$	$z$	Occupancy <sup>a</sup>		
					$T = 10$ K	$T = 293$ K	$T = 1273$ K
$P4/m$	1a	0	0	0	0.06(2)	0.13(2)	
	1b	0	0	1/2	0.45(2)	0.37(2)	
	1c	1/2	1/2	0	0.00(2)	0.01(2)	
	1d	1/2	1/2	1/2	0.23(2)	0.27(2)	
$I4/m$	2a	0	0	0			0.11(3)
	2b	0	0	1/2			0.30(2)

<sup>a</sup> Occupancies were refined assuming  $U_{iso} = 0.01 \text{ \AA}^2$  for  $T = 10$  K,  $U_{iso} = 0.015 \text{ \AA}^2$  for  $T = 293$  K and  $U_{iso} = 0.05 \text{ \AA}^2$  for  $T = 1273$  K. Standard uncertainties are given in parentheses.

a more constricted channel diameter at  $z = 0$  and can only accommodate approximately half as many additional Ni atoms.

### 3.5. Description of the structure

Alternating square networks of A atoms (filled circles) and B atoms (open circles), displaced with respect to one another as shown in figure 7(a), constitute the cubic B2-type crystal structure. Binary compounds of this type have an equiatomic composition (50% A atoms and 50% B atoms) assuming there are no vacant lattice sites. Deviations from the equiatomic composition can occur, however, when B atoms substitute for some of the A atoms (or vice versa) assuming that the unsubstituted networks remain filled. This type of substitution occurs in the tetragonal structure of the three compounds  $Zr_9Pt_{11}$ ,  $Zr_9Pd_{11}$ , and  $Zr_9Ni_{11}$  (45% Zr atoms and 55% Pt, Pd, or Ni atoms). The substituted Pt, Pd or Ni atoms (known as anti-site atoms) are located in the Zr-atom layers (filled circles) and are indicated by the letter 'a' in the open circles; each anti-site atom is surrounded by eight nearest-neighbor open circles and six, more distant, filled circles. These anti-site atoms form linear chains of alternating Zr and anti-site atoms perpendicular to the layers and parallel to the  $c$ -axis of the tetragonal structure. It is assumed that all atoms are confined to the planar networks. The linear atomic chains lie on the central axis of square prismatic columns formed by their neighboring atoms (figure 8(a)). Each linear chain is displaced by a translation of 1/2 along the tetragonal  $c$ -axis with respect to neighboring chains. In summary, this is a classical description of the  $A_9B_{11}$  structure.

This classical description of the structure fails to take into account the sizable lattice strains that are introduced when the relatively small Pt, Pd or Ni atoms are substituted for the significantly larger Zr atoms (using the metallic radii for CN = 12 [14], the atomic size difference between the anti-site atoms and a Zr atom is 13%, 14%, and 22%, respectively, for Pt, Pd, and Ni). Additional strain is introduced by strong chemical bonding that exists between the A (Zr) and B (M = Pt, Pd, Ni) atoms. These strains distort the classical structure so that the atomic networks are not evenly spaced (figures 8(b)–(d)) and they are no longer square (figure 7(b)). Each anti-site atom is now surrounded by six nearest-neighbor A atoms (filled circles) and eight more distant B atoms

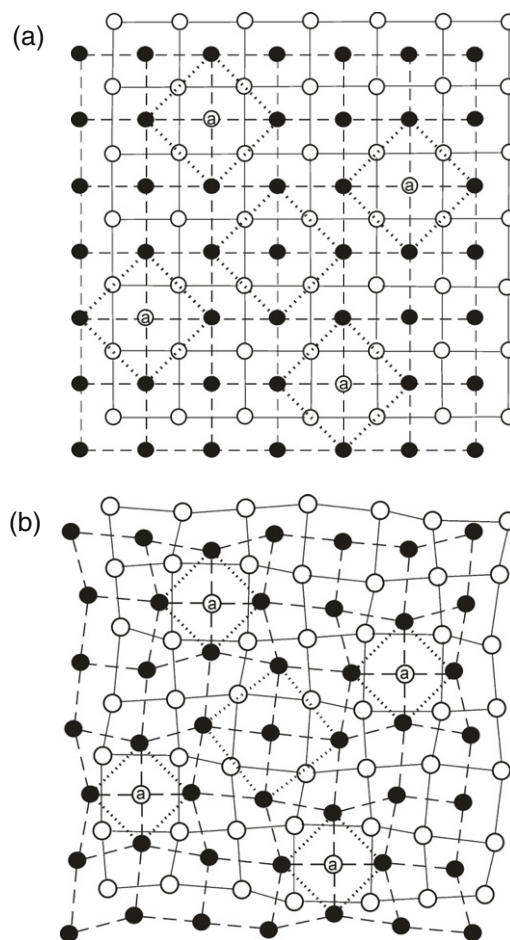


**Figure 7.** (a) Square networks of A atoms (filled circles) and B atoms (open circles) showing the location of anti-site atoms ('a' within the open circle) in the idealized  $A_9B_{11}$  tetragonal structure derived from the B2 structure type. The locations of the anti-site atoms are shifted by  $x, y = 1/2, 1/2$  in alternate A-atom networks. (b) Square networks of A atoms and B atoms as in (a), distorted as they are in the actual tetragonal structure of  $Zr_9Ni_{11}$ .

(open circles), an eversion of the idealized coordination shown in figure 7(a). The biggest departure from classical behavior, however, is the failure of the linear chain atoms to occupy fixed positions at all. Instead, we propose that they exist as strongly bonded pairs of Zr and anti-site atoms (figures 8(b), (c)) that can occupy numerous positions along the chain axes and seem to move rather freely over short distances. These atomic pairs are displaced by varying amounts from their classical positions within the layered networks. These displacements are not entirely random and are apparently determined by the presence of fixed atoms in the surrounding columns and by short-range interactions with neighboring atom chains. Additional M = Ni, Pd, Pt atoms may also be present along the chain axes (figure 8(d)).

The  $Zr_9M_{11}$  structure type thus consists of a tightly linked framework of Zr and M atoms, with relatively open channels along the fourfold axes. These channels at  $0, 0, z$  and  $1/2, 1/2, z$  are equivalent for the I-centered structure that exists for  $Zr_9Ni_{11}$  at  $1000^\circ\text{C}$  but differ at room temperature and below. Figure 9 presents a projection of the room-temperature

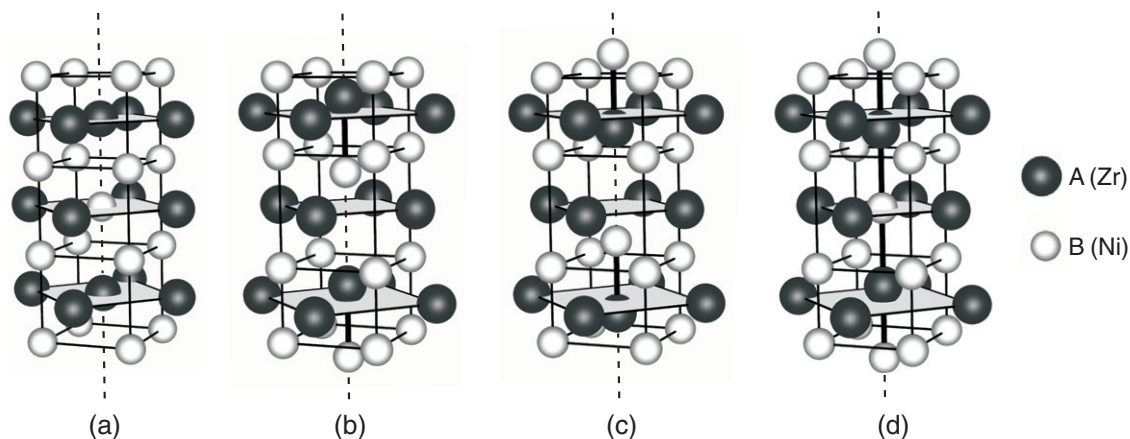


**Figure 8.** (a) Linear chains surrounded by prismatic columns in the idealized  $A_9B_{11}$  structure, assuming that all atoms are confined to planar networks. (b) Prismatic columns centered by A–B atomic pairs along the fourfold axis at  $x, y = 0, 0$  in the  $Zr_9Ni_{11}$  crystal structure. The crystallographic mirror planes are indicated by shaded rectangles. The atomic pairs are disordered off of the mirror planes, and have considerable range of static displacement along the fourfold axis. (c) Alternate orientation of the Zr–Ni atomic pairs. (d) One possible mechanism for the insertion of additional Ni atoms at  $z = 1/2$ .

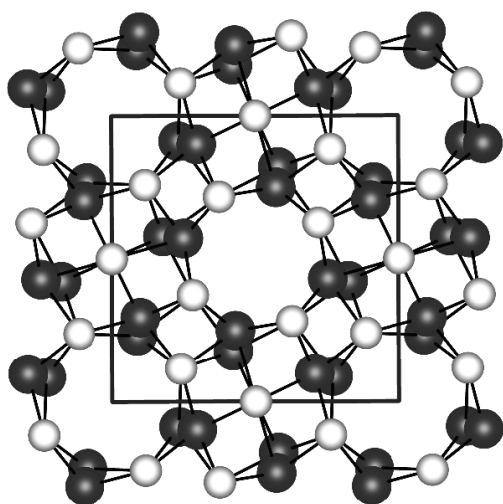


**Figure 9.** Projection of the  $Zr_9Ni_{11}$  structure along [001], including unit cell outline. The channels at  $x, y = 0, 0$  have a minimum radius of 2.581(5) Å while the channels at  $x, y = 1/2, 1/2$  have a minimum radius of 2.447(4) Å. Atoms within the channels have been omitted for clarity.

structure of  $Zr_9Ni_{11}$  along [001], showing the open channels. These channels are occupied by linear atomic chains that are largely uncorrelated with chains in adjacent channels although the atomic positions within the chains are not random with respect to the framework structure.

#### 4. Discussion

Whereas we cannot rule out other mechanisms to account for the apparent deviation from the ideal 9:11 composition, the stuffing of additional Ni atoms along the fourfold axes seems most likely. The average Zr–Ni distance along the chains of the idealized structure (Zr and Ni atoms on the mirror planes) is 3.304 Å, significantly longer than the distances of 2.6 to

**Table 5.** Framework interatomic distances for  $Zr_9Ni_{11}$  from neutron Rietveld refinement at room temperature. Standard uncertainties are given in parentheses.

Atoms	Distance (Å)	Atoms	Distance (Å)
Zr(3)–Zr(5)	3.288(6)	Zr(3)–Ni(3)	2.629(4) [ $\times 2$ ]
Zr(3)–Zr(5)	3.111(6)	Zr(3)–Ni(4)	2.664(4) [ $\times 2$ ]
Zr(3)–Zr(6)	3.368(1) [ $\times 2$ ]	Zr(3)–Ni(4)	2.589(4) [ $\times 2$ ]
Zr(4)–Zr(5)	3.378(1) [ $\times 2$ ]	Zr(3)–Ni(5)	2.776(4) [ $\times 2$ ]
Zr(4)–Zr(5)	3.236(6)	Zr(4)–Ni(3)	2.711(4) [ $\times 2$ ]
Zr(4)–Zr(6)	3.347(6)	Zr(4)–Ni(4)	2.701(3) [ $\times 2$ ]
		Zr(4)–Ni(5)	2.731(4) [ $\times 2$ ]
Ni(3)–Ni(3)	2.790(6)	Zr(4)–Ni(5)	2.628(4) [ $\times 2$ ]
Ni(3)–Ni(4)	2.811(2) [ $\times 2$ ]	Zr(5)–Ni(4)	2.658(4) [ $\times 2$ ]
Ni(4)–Ni(4)	2.772(4)	Zr(5)–Ni(5)	2.727(4) [ $\times 2$ ]
Ni(4)–Ni(5)	2.640(3)	Zr(5)–Ni(5)	2.797(4) [ $\times 2$ ]
Ni(5)–Ni(5)	2.686(4)	Zr(6)–Ni(4)	2.694(4) [ $\times 2$ ]
		Zr(6)–Ni(4)	2.782(4) [ $\times 2$ ]
		Zr(6)–Ni(5)	2.726(4) [ $\times 2$ ]

2.7 Å within the Zr–Ni framework (table 5) and those reported for other phases such as  $ZrNi$  [15] and  $Zr_7Ni_{10}$  [16, 17] near the equiatomic composition. It is thus possible spatially to insert extra Ni atoms in the large central cavity (figure 8(d) presents only one of many possible mechanisms); the insertion of additional Zr atoms would result in unacceptably short Zr–Zr distances. These Zr–Ni ‘rods’ most likely extend across the conventional unit cell; if an average Zr–Ni or Ni–Ni distance is assumed to be approximately 2.6–2.7 Å, then the unit cell can accommodate up to one extra Ni atom for every two unit cell lengths in the crystallographic  $c$  direction. This is consistent both with the refined atomic scattering density and the spacing of 2.64 Å (table 1) for the diffuse sheets observed in the SAED patterns. The two-dimensional modulation of intensity along the sheets observed in the SAED patterns indicates a weak correlation between atomic chains. The spacing of the diffuse sheets of intensity of 2.83 Å for  $Zr_9Pd_{11}$  and 2.88 Å for  $Zr_9Pt_{11}$  is also appropriate for Zr–M and M–M distances.

It should be noted that in the  $P4/m$  structure, the two channels at  $x, y = 0, 0$  and  $x, y = 1/2, 1/2$  are quite different. The minimum channel ‘diameter’ for  $x, y = 1/2, 1/2$  is much smaller than that for  $x, y = 0, 0$  and the refinements to determine scattering density (see table 4) indicate a lower occupation of additional Ni atoms. Whereas for the fourfold axis at  $x, y = 0, 0$  bond distance calculations indicate that a Ni atom could occupy any position along the axis, at  $x, y = 1/2, 1/2$  the occupation of the position at  $= 0$  would result in a Ni–Zr distance of 2.45 Å which is improbably short. Thus this axis at  $x, y = 1/2, 1/2$  can accommodate fewer additional Ni atoms than the axis at  $x, y = 0, 0$  and can be considered to be occupied by disordered Zr–Ni pairs of atoms that might shift sufficiently to add up to one additional Ni atom for every four unit cell distances along the  $c$  axis.

The proposed model also accounts for the irreproducibility of the neutron diffraction patterns on thermal cycling. Structure factor calculations indicate that the positions of the atoms along the fourfold axes strongly affect the intensity of the (420/240) reflection. The Ni and Zr atoms in the chains apparently move from one local energy minimum to another as the temperature is changed, resulting in large intensity changes in the neutron diffraction pattern. This movement occurred even between 4 and 10 K when the sample was cooled in a closed-cycle refrigerator. Repeat experiments did not result in consistent results, since the thermal cycling yields essentially a different starting sample for each experiment. These results also suggest the unusual situation that a unique structural state is not achieved even at low temperature, and that the thermodynamic states, including the ground state, may not be unique.

A similar type of linear disorder has been reported previously for other materials, for example the highly conducting compounds formed by oxidation of organic or organometallic compounds with elemental iodine or bromine [18–21]. In these materials the partially oxidized organic or organometallic molecules form columnar stacks which are surrounded by disordered polyhalide chains. The observed sheets of diffuse scattering from the polyhalide chains are in general incommensurate with the crystalline lattice. When the molecular framework causes constrictions in the polyhalide chains, the long-range order is disrupted and the diffuse x-ray scattering becomes broad and irregular which is indicative of short-range order (see Scaringe *et al* [22] and references therein). A similar example involving metal–metal chains has been reported for  $\text{Hg}_3\text{AsF}_6$  [23–25]. In this case the Hg atoms form two orthogonal non-intersecting chains, with a Hg–Hg distance of 2.64 Å indicated by the planes of diffuse scattering. The  $\text{Zr}_9\text{M}_{11}$  structures also present similarities with many zeolite structures, in that preferred atomic positions exist within the channels for adsorbed ions or molecules. In particular, it has been proposed that  $\text{Se}_2^{2-}$  dimers form linear chains within the channels of cancrinite; these chains were found to be incommensurate with the cancrinite lattice, and the arrangement of the dimers was found to be dependent on the temperature [26].

To our knowledge, this is the first report of incommensurate linear disorder for an intermetallic compound where

two dissimilar metals make up the disordered chains. It has been proposed that the Ru atoms occupying channels in the  $\text{Er}_3\text{Ru}_2$  structure are not coordinated with the rest of the structure [27]; such disorder has also been suggested for Ni atoms in  $\text{Pr}_{15}\text{Ni}_7\text{Si}_{10}$  [28] and Y atoms in  $\text{Y}_{13}\text{Pd}_{40}\text{Sn}_{31}$  [29]. The magnetic superconductor  $\text{Y}_9\text{Co}_7$ , in which the Co atoms are disordered along the sixfold symmetry axis in the space group  $P6_3/m$ , is perhaps the most similar material reported to date [30, 31]. A ‘hopping’ mechanism has been proposed for the unusual temperature dependence of the magnetism and conductivity in  $\text{Y}_9\text{Co}_7$  [32, 33]. Yvon *et al* [31] predicted but were unable to observe diffuse x-ray scattering for this structure; such weak diffuse scattering is usually difficult to detect by x-ray or neutron diffraction but is readily observed in electron diffraction. We have in fact observed diffuse scattering similar to that for the  $\text{Zr}_9\text{M}_{11}$  compounds in SAED patterns of  $\text{Y}_9\text{Co}_7$ , which will be discussed elsewhere.

In summary, we have combined transmission electron microscopy with neutron powder diffraction to probe the structure and unusual diffuse scattering of the tetragonal intermetallic compounds  $\text{Zr}_9\text{M}_{11}$  ( $\text{M} = \text{Ni}, \text{Pt}, \text{Pd}$ ). The composition was found to be  $\text{Zr}_9\text{M}_{11+\delta}$  ( $\delta \approx 0.4$ ). These materials have a host periodic structure, which was found to have a primitive rather than body-centered lattice at room temperature, as well as structurally disordered one-dimensional chains of atoms that are only weakly correlated with each other. The diffuse scattering from these chains results in two-dimensional sheets of intensity in reciprocal space with translations which are in general incommensurate with the translations of the host lattice. These parallel sheets have a spacing that is appropriate for Zr–M and/or M–M distances. The atoms within the chains move rather freely down to 4 K, with no apparent unique structural state, and it is possible that these chains could impose special one-dimensional properties within the periodic host structure.

## Acknowledgments

We thank Dr Klaus Yvon for his helpful suggestions, and Dr Radovan Černý and Dr Jean-Marc Joubert for kindly supplying us with additional information.

*Note added in proof.* After the initial submission of this manuscript, it was brought to our attention that Černý and Joubert [34] have postulated a similar model for the incorporation of additional Ni atoms along the fourfold axes in  $\text{Zr}_9\text{Ni}_{11+\delta}$  based upon single-crystal x-ray diffraction data. Although detailed structural results were not presented, their model is in essential agreement with that proposed herein.

## References

- [1] Hermann C 1931 *Z. Kristallogr.* **79** 186
- [2] Mabis A J 1962 *Acta Crystallogr.* **15** 1152
- [3] Panda S C and Bhan S 1973 *Z. Metallkd.* **64** 793
- [4] Kirkpatrick M E and Larsen W L 1961 *Trans. Am. Soc. Met.* **54** 580
- [5] Glimois J L, Beclé C, Develey G and Moreau J M 1979 *J. Less-Common Met.* **64** 87
- [6] Shadangi S K, Panda S C and Bhan S 1982 *Acta Crystallogr. B* **38** 2092

- [7] Waterstrat R M, Shapiro A and Jeremie A 1999 *J. Alloys Compounds* **290** 63
- [8] Bendersky L A, Stalick J K and Waterstrat R M 1993 *J. Alloys Compounds* **201** 121
- [9] Bendersky L A, Stalick J K, Portier R and Waterstrat R M 1996 *J. Alloys Compounds* **236** 19
- [10] Larson A C and Von Dreele R B 2005 General structure analysis system (GSAS) *Los Alamos National Laboratory Report* LAUR 86-748
- [11] Stalick J K and Waterstrat R M 2007 *J. Alloys Compounds* **430** 123
- [12] Marcinkowski M J and Brown N 1961 *Acta Metall.* **9** 764
- [13] Joubert J M, Latroche M and Percheron-Guégan A 1995 *J. Alloys Compounds* **231** 494
- [14] Pearson W B 1972 *The Crystal Chemistry and Physics of Metals and Alloys* (New York: Wiley-Interscience) p 151
- [15] Kirkpatrick M E, Bailey D M and Smith J F 1962 *Acta Crystallogr.* **15** 252
- [16] Joubert J M, Černý R, Yvon K, Latroche M and Percheron-Guégan A 1997 *Acta Crystallogr. C* **53** 1536
- [17] Kirkpatrick M E, Smith J F and Larsen W L 1962 *Acta Crystallogr.* **15** 894
- [18] Endres H, Keller H J, Megnamisi-Belombe M, Moroni W, Pritzkow H, Weiss J and Comès R 1976 *Acta Crystallogr. A* **32** 954
- [19] Herstein F H, Kapon M and Reisner G M 1981 *Proc. R. Soc. A* **376** 301
- [20] Kawamoto T, Mori T, Uji S, Yamaura J I, Kitagawa H, Takamori A, Takimiya K and Otsubo T 2005 *Phys. Rev. B* **71** 172503
- [21] Phillips T E, Scaringe R P, Hoffman B M and Ibers J A 1980 *J. Am. Chem. Soc.* **102** 3435
- [22] Scaringe R P, Pace L J and Ibers J A 1982 *Acta Crystallogr. A* **38** 608
- [23] Brown I D, Cutforth B D, Davies C G, Gillespi R J, Ireland P R and Vekris J E 1974 *Can. J. Chem.* **52** 791
- [24] Hastings J M, Pouget J P, Shirane G, Heeger A J, Miro N D and MacDiarmid A G 1977 *Phys. Rev. Lett.* **39** 1484
- [25] Schultz A J, Williams J M, Miro N D, MacDiarmid A G and Heeger A J 1978 *Inorg. Chem.* **17** 646
- [26] Poborchii V V, Sato M and Shchukarev A V 1997 *Solid State Commun.* **103** 649
- [27] Fornasini M L and Palenzona A 1990 *Z. Kristallogr.* **192** 249
- [28] Hovestreydt E and Parthé E 1985 *Acta Crystallogr. C* **41** 310
- [29] Cenžual K and Parthé E 1984 *Acta Crystallogr. C* **40** 1127
- [30] Kolodziejczyk A, Leciejewicz J, Szytula A, Chmista J and Wegrzyn J 1987 *Acta Phys. Pol. A* **72** 319
- [31] Yvon K, Braun H F and Gratz E 1983 *J. Phys. F: Met. Phys.* **13** L131
- [32] Sarkissian B V B 1985 *J. Appl. Phys.* **57** 3203
- [33] Sarkissian B V B 1986 *J. Phys. F: Met. Phys.* **16** 755
- [34] Černý R and Joubert J M 1998 *Mater. Struct. Chem., Biol. Phys. Technol.* **5** 377